Catalysis Letters (2022) 152:781–790
https://doi.org/10.1007/s10562-021-03667-9

Ionic Liquids Grafted Mesoporous Silica for Chemical Fixation of CO_2 to Cyclic Carbonate: Morphology Effect

Jie Yao[1] · Mengdi Sheng[1] · Shiyang Bai[1] · Hongjing Su[1] · Hui Shang[1] · Han Deng[1] · Jihong Sun[1]

Received: 8 February 2021 / Accepted: 16 May 2021 / Published online: 25 May 2021

Abstract

Three mesoporous silica materials (MCM-41, MSN and BMMs) possessing different morphologies but similar hexagonal arranged mesopores with almost the same pore size (2–3 nm) were functionalized by Zn and [1-(trimethoxysilyl)propyl-3-methylimidazolium] ionic liquid (ILs) via post-grafting treatment. The ILs grafted mesoporous silicas were then characterized by porosity, microscopy and SAXS techniques, and the successful loading of Zn and ILs, as well as the different distribution of functional groups in different supports were shown. Furthermore, the cycloaddition reaction of CO_2 with epoxide was employed to evaluate the influences of the ILs distribution, which was proved to be caused mainly by varying morphologies of different supports. All the catalysts showed good catalytic activities. Interestingly, at low temperature, the inter particle supported ILs in BMMs had the highest catalytic efficiency, while the aggregation grafting ILs on MCM-41 present the lowest activity. However, the mesoporous silicas with ordered arranged nanopores present the superiority at higher temperature. The results highlight the crucial role played by the morphology of the supports.

Graphical abstract

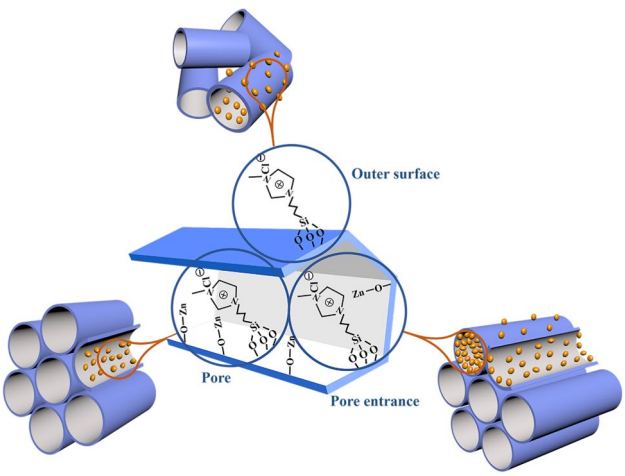

Keywords Mesoporous silicas · Ionic liquids · Morphology effect · Carbon dioxide · Cyclic carbonate

1 Introduction

Porous materials refer to the existence of interpenetrating or closed pores inside the material [1]. The materials research spanned the wider fields covered by adsorption, separation, catalysis and electrochemistry [2]. Porous supports are well received in catalytic science for many reasons, such

✉ Shiyang Bai
sybai@bjut.edu.cn; jhsun@bjut.edu.cn

[1] Beijing Key Laboratory for Green Catalysis and Separation, Department of Environmental and Chemical Engineering, Beijing University of Technology, 100 PingLeYuan, Chaoyang District, Beijing 100124, People's Republic of China

as high specific surface area, well-developed channels that allow the diffusion of small molecules, and many pores that can accommodate a variety of catalysts. Ionic liquids (ILs), which have been widely applied as catalyst for a variety of chemical reactions [3, 4], are one of the good candidates to be hosted inside the pores of those materials. Because ILs have a number of favorable advantages, such as near-zero vapor pressure, high thermal stability, wide electrochemical window, and tunable properties [5, 6], but their crucial disadvantage lies in the difficulty in product separation and purification, as well as difficult recycling, restrict the development of catalysis. To solve these problems, immobilization of ILs into some solid supports thereafter serving as heterogeneous catalysts for the reactions is considered as one of the simplest methods.

Many porous materials have been used to load the ILs, such as mesoporous silica [7, 8], polymers (e.g. polystyrene resin) [9, 10], graphene oxide (GO) [11, 12] and montmorillonite [13]. Among these supports, the mesoporous silica materials have received much attention because of their large surface areas, uniform ordered mesoporous channels, high hydrothermal stability, easy functionalized surfaces property and tunable pore dimension and channel structure [14–16]. They have been used in many reactions as the support of ILs to achieve the easy separation and recycle of ILs. In order to heterogenized the active center into the mesoporous silica, there are three main strategies [17, 18], including grafting, co-condensation, and confinement. Due to the special functional groups in ILs, which may affect the acidity and basicity of the synthesis system, grafting is the most common and effective method for immobilizing ILs. It is well known that the disadvantages of nonhomogeneous distribution of the organic groups and a lower degree of occupation within the pores, which will influence the accessibility and dispersion of the active center, are the main drawback of grafting. Therefore, the nanopores of these mesoporous supports can influence the catalytic reaction process [19, 20], resulting in the different catalytic performances. Take SBA-15 and a non-porous amorphous silica as an example, NBu_4I + SBA-15 exhibited 2.7 times higher activity than $NBu_4I + SiO_2$ in the cycloaddition of CO_2 with styrene oxide [21], due to the regular concave curved morphology of SBA-15 which might provide a favorable geometry for the cooperative interactions of Si–OH and halide. Moreover, the pore size of silica was found to be important for catalysis [22, 23], and mesoporous silica with larger mean pore size presented much better performance than that with smaller pore. The pore structure of the support is another key factor that must be considered [24, 25], as the catalytic activity depended on the structure of the support strongly. Also, in our previous research [26], abundant microporous structure in mesoporous support make a great contribution to reducing mass transfer resistance, therefore enhancing the activity of immobilized ILs. However, to the best of our knowledge, the intensive research about the combined effect of different morphology of mesoporous materials with the same pore channels have seldom been systemically investigated.

Herein, the simplest supported method of grafting was employed to immobilize imidazolium salt ionic liquids [1-(trimethoxysilyl)propyl-3-methylimidazolium chloride] into different mesoporous silicas to fabricate the heterogeneous ILs, thereby using as catalysts in the cycloaddition of CO_2 with epoxide, whose atom economy is 100%. And such products have received increasing attention due to their application in various industrial process, such as precursors of pharmaceuticals, polar aprotic solvents, and intermediates in the synthesis of polycarbonates [27–29]. Moreover, ILs is one of the most attractive catalysts in this reaction, although a wide range of catalysts can be used to promote these transformations. The supports used in this work have the same mesoporous structure of a hexagonal arrangement of the mesopores and space group of p6mm, including MCM-41 [30], MSN [31], and BMMs [32]. The supports and the synthesized catalysts were characterized by various techniques and the question of accessibility to the active center was addressed by means of N_2 adsorption and SAXS. Moreover, the effects of reaction parameters including the reaction temperature, and CO_2 pressure were investigated to further demonstrate the influences of morphologies of different supports on the catalytic activities.

2 Experimental Section

2.1 Chemicals

Cetyltrimethyl ammonium bromide (CTAB, 99%), tetraethyl orthosilicate (TEOS, 98%), 3-chloropropyltrimethoxysilane (98%), N-methylimidazole (99%), propylene oxide (PO, 99.5%), propylene glycol (PG, 99.5%), biphenyl (99.5%) and propylene carbonate (PC, 99.5%) were obtained from J&K-Balcony Reagents. NaOH, $NH_3{\cdot}H_2O$ (25%), toluene, ether, anhydrous methanol and ethanol were purchased from Beijing chemical works. Zinc acetate (99.99%) were obtained from Aladdin. All of the solvents and reagents were of AR. Deionized water is self-made in the laboratory.

2.2 Characterization

The FT-IR spectra were measured by a Germany Bruker Tensor-27 analyzer. SEM microscopy was performed on a Japan S-4300 field emission scanning electron microscope and TEM micrographs were taken using a Japan JEOL JEM-1200EX transmission electron microscope at 200 kV. The N_2 adsorption/desorption isotherms were performed at − 196 °C using an America Micromeritics Tristar II 3020

analyzer. All samples were previously outgassed at 80 °C for 6 h before measurements. Specific surface areas of each material were calculated by Brunauer-Emmett-Teller (BET) model, the plots of the corresponding pore size distribution were calculated from the N_2 adsorption branches with the Barrett-Joyner-Halenda (BJH) model. The total pore volumes were estimated from the amounts adsorbed at a relative p/p_0 of 0.99. The powder X-ray diffraction (XRD) measurement was carried out with a Germany Bruker-AXS D8 Advance X-ray diffractometer using Cu Kα radiation ($\lambda = 0.154$ nm) within the scattering angel 2θ range of 1–10° and 10–50°at 36 kV and 20 mA. The metal contents of the catalysts were tested by an America PerkinElmer Optima 7000DC inductively coupled plasma optical emission spectrometer (ICP). Elemental analysis (EA) was carried out using Germany LECO CHN628. The SAXS experiments were performed using synchrotron radiation as the X-ray source at the 1W2A station at the Beijing Synchrotron Radiation Facility. The incident X-ray wavelength was 0.154 nm. The sample-to-detector distance was 1565 mm and was calibrated by using the diffraction ring of a standard sample. The scattering vector magnitude q ($q = 4\pi\sin\theta/\lambda$ where 2θ is the scattering angle) ranged from 0.08 to 2.34 nm^{-1} for the experiment reported in this paper. The detector readout noise (dark current) of the detector, measured with a mask before the sample measurements, was approximately 10 counts s^{-1} for the Mar165 CCD. The sample was loaded into a sample cell and sealed with Scotch tape on a groove. The thickness of the sample cell was approximately 1 mm.

2.3 Preparation of Zn Functionalized Hexagonal Mesoporous Silicas (H-MS)

CTAB (2.5 g), distilled water (120 mL) and $NH_3{\cdot}H_2O$ (9.5 mL) were mixed in the flask. After stirring several minutes, TEOS (10 g) was added drop by drop. The mixture was stirring at room temperature for 1 h. After that, the mixture was transferred to stainless steel autoclave at 130 °C for 72 h, and then filtrated, subsequently dried overnight under 80 °C. To remove the surfactant, the powder was subjected to calcination in air for 5 h at 540 °C (heating rate: 1 °C min^{-1}) to obtained MCM-41.

CTAB (0.5 g) was added to a 500 mL flask containing distilled water (240 mL) with slow stirring and NaOH (1.5 mL, 2 mol/L) was added to this solution. When the temperature was heated to 80 °C, TEOS (2.5 mL) was added to the mixture dropwise. The mixture was stirred for 2 h and filtrated to obtain the white solid. Then it was heated at a rate of 1 °C min^{-1} to 500 °C for 6 h to obtained MSN.

CTAB (2.0897 g) was dissolved in distilled water (83.2 mL) and stirred at 40 °C to obtain homogeneous mixture and TEOS (6.4 mL) and $NH_3{\cdot}H_2O$ (1.92 mL) was added to this solution with rapid stirring. After a few minutes, the mixture turned into a white gel gradually. This gel was filtered and washed with distilled water. Then, the dried solid was heated at a rate of 5 °C min^{-1} to 550 °C for 6 h to remove the surfactant and a dry BMMs was obtained.

0.5 g calcined mesoporous silicas (MCM-41, MSN, BMMs) were treated at 120 °C under vacuum for 3 h to remove physical absorbed water and were cooled to room temperature under a N_2 atmosphere. Then, 50 mL $Zn(OAc)_2{\cdot}2H_2O$ solution was added into the flask and was stirred for 10 h at room temperature. The powder was washed several times with ethanol and distilled water to remove excess zinc acetate. Finally, MCM-41/Zn, MSN/Zn, BMMs/Zn were obtained.

2.4 Preparation of Immobilized ILs on Mesoporous Silica

The ILs was prepared by the method reported previously [33]. 3-chloropropyltrimethoxysilan (20 mL) and N-methylimidazole (8.2 mL) was mixed in a flask, and the mixture was stirred for 24 h under a N_2 atmosphere. Then, the mixture was washed for three times with ether to remove unreacted excess reactants. The ether was removed by evaporation. Finally, viscous and light yellow ionic liquids were obtained and denoted as ILs.

0.5 g MCM-41/Zn, MSN/Zn, and BMMs/Zn were treated at 100 °C under vacuum for 3 h. Then heated to 110 °C, toluene (30 mL) and ILs (200 μL) were added. After refluxing for 12 h, the powder was centrifugal with ethanol, and dried overnight. Finally, the catalysts were denoted as MCM-41/Zn-ILs, MSN/Zn-ILs, BMMs/Zn-ILs.

2.5 Catalytic Reactions

The cycloaddition of CO_2 with PO was carried out in 50 mL stainless steel autoclave with stirring. In a typical reaction process, catalyst and 8 mL PO (S/C = 200, S/C = Moles of PO/Moles of catalyst) were added into the reactor. The reaction was carried out with a present pressure of carbon dioxide (0.5–1.5 MPa) at a different temperature (80–120 °C). After stirring for 8 h, the reactor was put into iced water to the room temperature. The obtained products were analyzed using a gas chromatograph (GC79000) equipped with DB-WAX capillary column and FID detector. The liquid mixture consisted of PO, PC, and 1, 2-propylene glycol (PG) as the byproduct originating from the hydrolysis of PO with trace H_2O. No other substance was detected.

3 Results and Discussions

According to our previous research, bifunctional solid catalysts containing both imidazolium salt ionic liquids (imi-ILs) and Zn(II) can efficiently promote the catalytic performance for this chemical fixation of CO_2 with epoxide [34].

Therefore, the preparation of H-MS (MCM-41, MSN and BMMs) supported ILs are based on the functionalization of the silica surface with Zn(II) (Scheme 1).

3.1 Characterization of the Catalysts

The FT-IR spectra of related samples are depicted in Fig. 1. The bands at 1085 cm^{-1}, 960 cm^{-1} and 800 cm^{-1} were ascribed to the asymmetric stretching vibrations of Si–O–Si, bending vibrations of Si–OH and symmetrical stretching vibrations of Si–O–Si [35], respectively. After Zn (Fig. 1b) and ILs (Fig. 1c) grafting, the relative intensity of the peak at 960 cm^{-1} was weakened gradually and vanished entirely. This result was consistent with previous report and further verified the successfully grafting of Zn and ILs through the condensation with Si–OH on the surface. Additionally, after immobilization of Zn (Fig. 1b), a new band at 1560 cm^{-1} appeared, which can be assigned to the C=O vibrations of zinc acetate [36]. Also, unlike pure mesoporous silicas, a small peak was observed at 1575 cm^{-1} after immobilization of ILs, which can be assigned to the C–H and C=N vibrations of imidazole rings [35]. Because the two peak positions are similar, there is no obvious difference.

The morphology and pore structure were characterized by SEM and TEM as shown in Fig. 2. The three H-MS have different morphologies. MCM-41/Zn-ILs (Fig. 2A-a) presents a bulky morphology with an average diameter of around 800 nm. And, MSN/Zn-ILs (Fig. 2A-b) which has a well dispersed nanosphere morphology, shows a particle size of about 80–100 nm. Although BMMs has an approximate spherical shape (~ 50 nm), the sample particle exhibits an aggregated dispersion. In the transmission electron micrographs of Fig. 2B, it is observed that well-ordered mesoporous structures with alternating channels can be seen for MSN/Zn-ILs and MCM-41/Zn-ILs, while BMMs/Zn-ILs presents a large number of narrow small pores around 2.6 nm. These data are in a good agreement with the results from nitrogen adsorption/desorption and XRD.

Porosity properties of all the as-synthesized materials were studied by nitrogen adsorption (Fig. 3 and Table 1). The N_2 adsorption–desorption curves of all samples featured the characteristics of type IV, accompanied by H1 hysteresis loops in the relatively medium-pressure region and H4 hysteresis loops in the relatively high-pressure region [37, 38]. In the relatively medium-pressure region, the turning point, which is related to the pore size distribution [38] indicates that the pore size distribution of

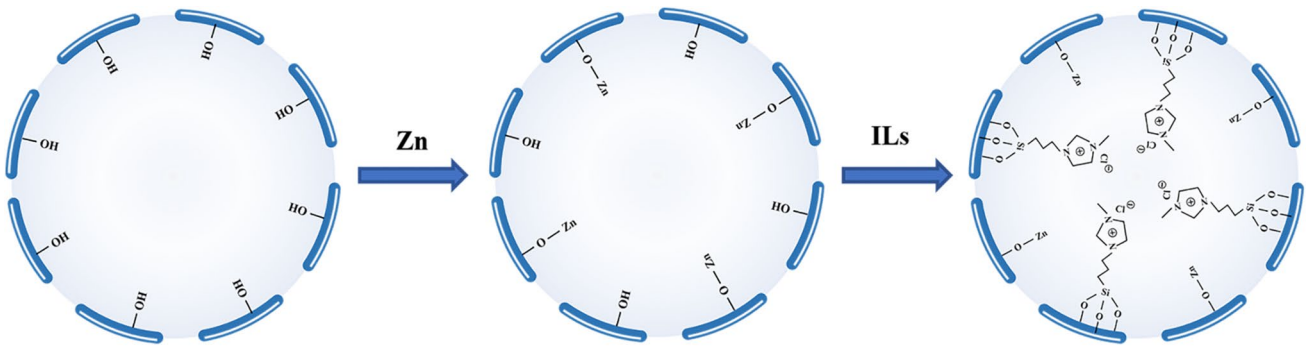

Scheme 1 Schematic diagram of heterogeneous catalyst synthesis

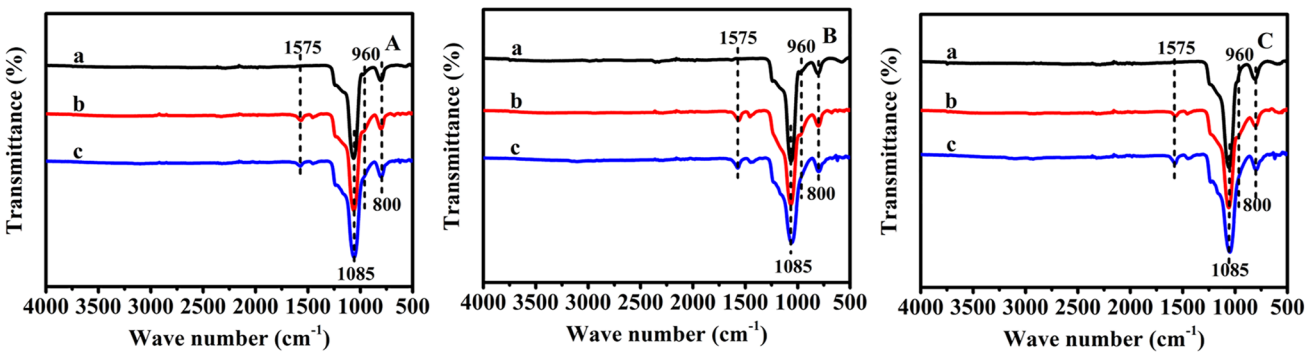

Fig. 1 FT-IR spectra of **A** MCM-41, **B** MSN and **C** BMMs series samples: **a**) H-MS, **b**) H-MS/Zn and **c**) H-MS/Zn-ILs

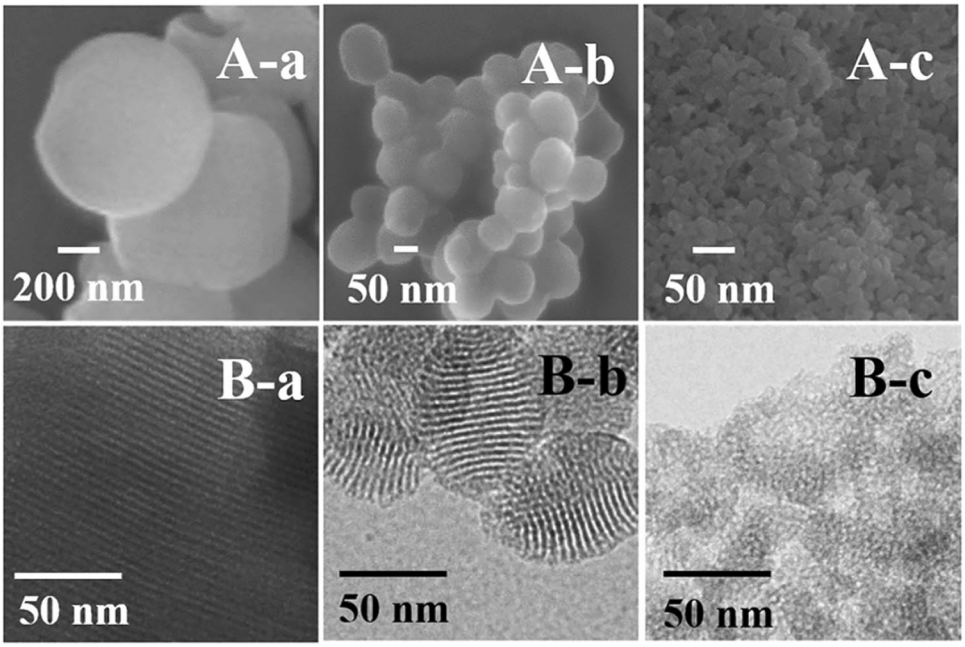

Fig. 2 **A** SEM and **B** TEM micrographs of **a**) MCM-41/Zn-ILs, **b**) MSN/Zn-ILs and **c**) BMMs/Zn-ILs

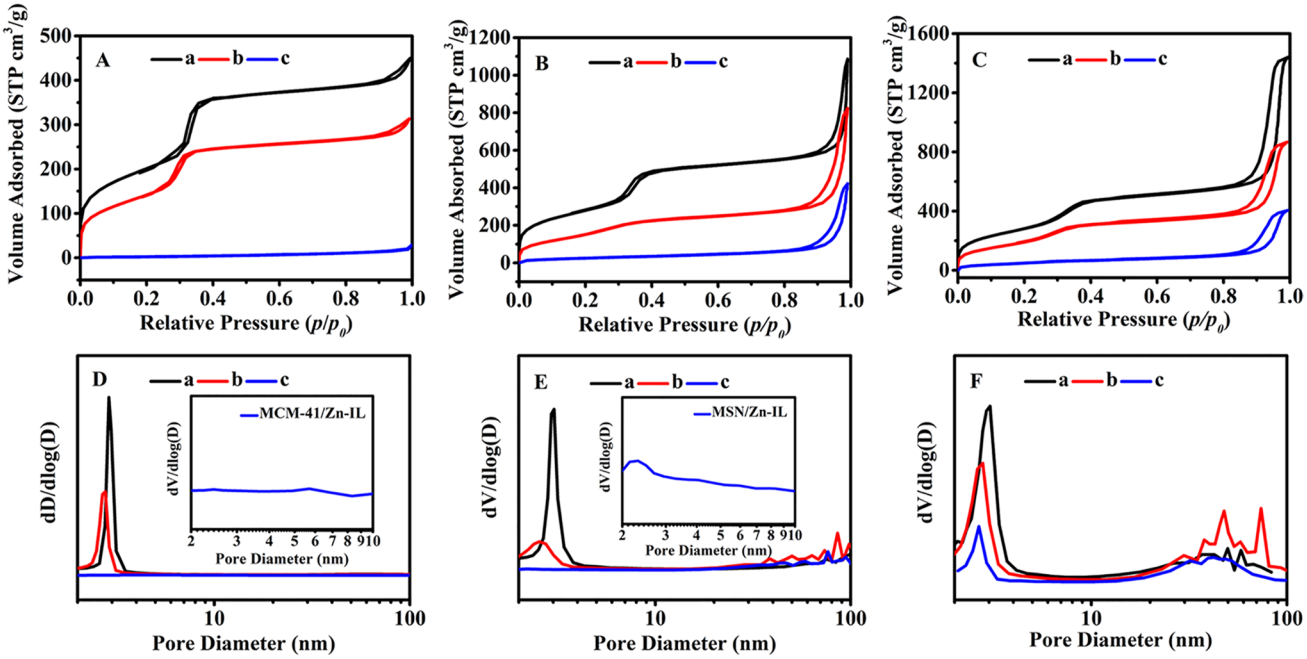

Fig. 3 N_2 adsorption/desorption isotherms and corresponding pore size distributions of **A**, **D** MCM-41, **B**, **E** MSN and **C**, **F** BMMs series samples: **a**) H-MS, **b**) H-MS/Zn and **c**) H-MS/Zn-ILs

the mesoporous silicas was narrow, and the pore sizes were mainly 2–3 nm (Fig. 3 and Table 1). The MSN and BMMs show the broad large pore distribution around 30–100 nm, which is originated from the accumulation of the spherical particles. And it is easy to find that the surface area, pore size, and pore volume all declined after Zn and ILs loading, due to the occupancy of pores by the functional groups. And it is noteworthy that the samples with immobilized Zn and ILs except MCM-41/Zn-ILs still remain open channels and enough surface areas, although the pore size distribution decreased. However, the surface area of MCM-41/Zn-ILs is relatively small. This can be assigned to a partial blockage of the pores by ILs; the accessibility of N_2 molecules is thus decreased, which can ultimately lead to a loss in catalytic efficiency. Along with the result of XRD as shown in Fig. S2, this is a strong

Table 1 Structural parameters and textural properties of all samples

Samples	BET surface area[a] ($m^2\ g^{-1}$)	Pore volume[b] ($cm^3\ g^{-1}$)	Small mean pore[c] (nm)
MCM-41	727.1	0.78	2.9
MCM-41/Zn	569.8	0.58	2.8
MCM-41/Zn-ILs	11.6	0.05	–
MSN	1022.4	1.82	3.0
MSN/Zn	629.9	1.36	2.6
MSN/Zn-ILs	99.9	0.68	2.3
BMMs	1048.5	2.21	2.9
BMMs/Zn	820.7	1.48	2.7
BMMs/Zn-ILs	325.7	0.69	2.7

[a]The BET surface area was calculated in a relative pressure range $p/p_0 = 0.05–0.3$

[b]Estimated from the amounts adsorbed at relative pressure (p/p_0) of 0.99

[c]The pore size distribution was calculated from the N_2 adsorption branch using the BJH method

Table 2 Amount of ILs and Zn measured from EA and ICP

Samples	EA (wt%)			ILs (mmol g^{-1})	Zn (mmol g^{-1})
	C	N	H		
MCM-41/Zn-ILs	15.48	3.70	2.38	1.3	0.9
MSN/Zn-ILs	17.17	4.43	2.68	1.6	1.2
BMMs/Zn-ILs	10.33	3.18	2.40	1.1	1.9

evidence to prove the maintained structure of the support and the successful immobilization of ILs. As, the XRD pattern of MSN, MCM-41 and BMMs display a strong diffraction peak around 2.0° which is the characteristic peak of mesoporous structure [32, 39, 40] and the peak can still be observed after functionalization of Zn and ILs, though the peak intensity decreases. The two weaker diffraction peaks near 4° for MSN and MCM-41 correspond to diffraction surfaces (110) and (200), respectively, indicating that the synthesized mesoporous silica has a high degree of internal order and belongs to a hexagonal close-packed structure. But BMMs only exhibited the (100) reflection peak, because of its poor-ordered mesoporous structure, just as shown in TEM image.

The content of Zn and ILs in the catalysts was analyzed by ICP and EA, respectively (Table 2). The weight percent of ILs could be obtained according to the content of N. Obviously, BMMs/Zn-ILs has the highest grafting amount of Zn but the lowest content of ILs (1.1 mmol g^{-1}). However, MSN/Zn-ILs, who owns the moderate Zn content, shows the highest loading of ILs (1.6 mmol g^{-1}). The catalysts were prepared through two steps including Zn grafting and ILs immobilizations (Scheme 1). In the first step, the amount of Zn loading in support follows the order of BMMs > MSN > MCM-41, which is also the order of the surface area and pore volume but opposite from the channel length order. This result is mainly caused by the differences of the utilizability and accessibility of the Si–OH on different supports. Moreover, Zn and ILs were all loaded through condensation with the Si–OH of the supports, therefore the amount of grafting between these two groups is competitive. In the second synthesis process, ILs were loaded in the Zn functionalized H-MS, whose surface Si–OH have already been occupied by Zn partly. So, BMMs/Zn-ILs who owns the highest Zn loading, shows the lowest ILs content. But, MCM-41/Zn-ILs, possessing the lowest Zn content, only has moderate ILs loading. This occurs because the long pore channel, low surface area and pore volume of MCM-41/Zn-ILs, which is mainly caused by the bulky morphology compare with other two H-MS used here.

Interesting information related to the microstructure changes of samples can be obtained on the SAXS results as shown in Fig. 4 and Table 3. Each curve was linearly fitted according to the least square method, and related parameters are obtained, including fractal dimension (D) and linear range. The results are listed in the Table 3. As can be seen in figures, in the lower scattering vector q, each scattering curve showed a good linear relationship with the

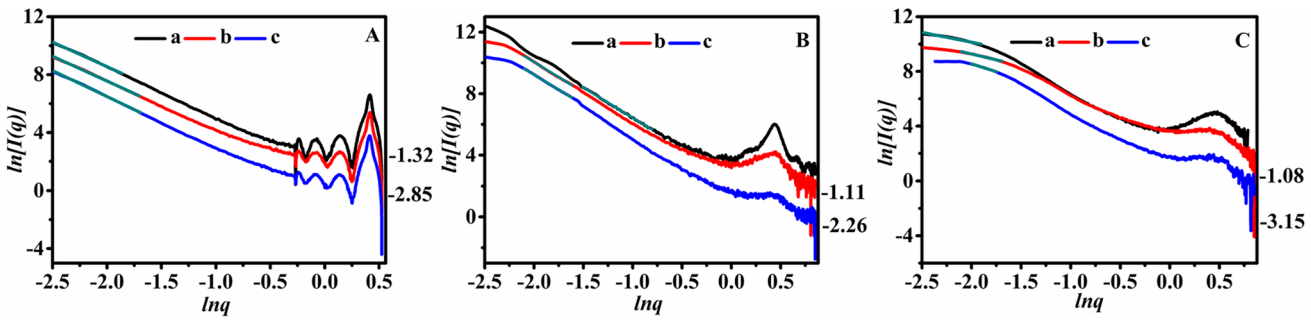

Fig. 4 Shifted scattering curves of **A** MCM-41, **B** MSN and **C** BMMs series samples: **a**) H-MS, **b**) H-MS/Zn and **c**) H-MS/Zn-ILs

Table 3 *D* values and linear range of all samples

Samples	*D* values	Linear range (nm^{-1})
MCM-41	2.61 (D_s)	$0.08 < q < 0.16$
MCM-41/Zn	2.54 (D_s)	$0.08 < q < 0.16$
MCM-41/Zn-ILs	2.38 (D_s)	$0.08 < q < 0.16$
MSN	2.05 (D_s)	$0.22 < q < 0.45$
MSN/Zn	2.05 (D_s)	$0.12 < q < 0.20$
MSN/Zn-ILs	2.09 (D_s)	$0.12 < q < 0.20$
BMMs	1.43 (D_m)	$0.08 < q < 0.15$
BMMs/Zn	1.71 (D_m)	$0.12 < q < 0.18$
BMMs/Zn-ILs	2.20 (D_m)	$0.14 < q < 0.17$

linear correlation coefficient $R^2 > 0.96$. Slopes between − 3 and − 4 are characteristic of a surface fractal (the surface fractal dimension, $2 < D_s < 3$) [41]. The result indicates that all samples have typical fractal characteristics. If the fractal slope is − 4, the surface is smooth (the surface fractal dimension equals 2 when a surface is non-fractal and completely smooth on the appropriate length scale) [42], between $D_s = 2$–3 the surface fractal is the characteristic, while between $D_m = 1$–3 the determinative is the mass fractal. Slopes from − 1 to − 3 indicate mass fractal structures (the mass fractal dimension, $1 < D_m < 3$). As the mass fractal increases, the structure of the species becomes more compact, when $D_m = 3$, it represents the Euclidean (nonfractal) [43]. For MCM-41, the gradually decreased surface fractal dimension after Zn and ILs loading has been attributed to the smoothening of the surface due to the grafting procedure, which mainly take place on the outer surface and pore entrance because of the long pore channel and bulky morphology of the support. The results are in reasonable agreement with those calculated from the N_2 adsorption isotherms. However, comparing the *D* values of MSN, MSN-Zn and MSN/Zn-ILs, it is found that although the surface fractal dimension gradually increases, the change is relatively small. Combined with the decrease of peak intensity, it can be concluded that Zn and ILs are mainly grafted inside the channels of MSN. Due to the aggregation of BMMs particles, there are a large number of accumulated pores on the surface. Mass fractal dimensions (D_m) have been obtained for BMMs series and the values are 1.43, 1.71 and 2.20 for BMMs, BMMs/Zn and BMMs/Zn-ILs respectively. The increased D_m, indicating a compacting of the pore surface interface due to the grafting of Zn and ILs. Combined with previous results of EA, TEM and N_2 adsorption, the distributions of active centers in different supports are summarized in Scheme 2: The longer pore channel of MCM-41 blocks the diffusion of functional groups, which makes the pore entrance and outer surface occupied, thereafter causing the blockage of the pore. On the contrary, the spherical morphology with the particle size of 80–100 nm for MSN is in favor of the immobilization of functional group into the nanopore instead of the outer surface or the pore entrance. And, in BMMs, which has wormlike mesoporous and a large number of accumulated pores, the functional groups distribute both inside the short pore channel and the inter-particle pores. The different distribution of ILs in different supports will dramatically affect the accessibility of the active center, thereby affecting their catalytic activity as catalysts.

3.2 Catalytic Properties of Different Kinds of Mesoporous Immobilized Catalysts

In the cooperative catalytic process, Zn acted as Lewis acidic coordinates with oxygen atom of epoxides [44]. The halide anion of ILs makes a nucleophilic attack on the less sterically anion carbon atom of epoxide [45]. Therefore, ILs, especially in cooperation with Zn, have been proved to be one of the most efficient catalysts for this cycloaddition reaction. Therefore, to evaluate the influences of different supports, the H-MS supported ILs catalysts were used in the cycloaddition of CO_2 with epoxide and the results are summarized in Table 4 and Fig. 5.

The catalytic activity of H-MS/Zn-ILs was evaluated in the cycloaddition of CO_2 with epoxide at 100 °C and 1.25 MPa for 8 h (Table 4). As expectation, different morphologies with the same pore sizes showed a big difference in catalytic performance. MCM-41/Zn-ILs showed the lowest yield of 33%, while the yield of MSN/Zn-ILs and BMMs/Zn-ILs were similar, about 76% and 77% respectively. The

Scheme 2 Schematic illustration of the distribution of functional groups in different mesoporous materials

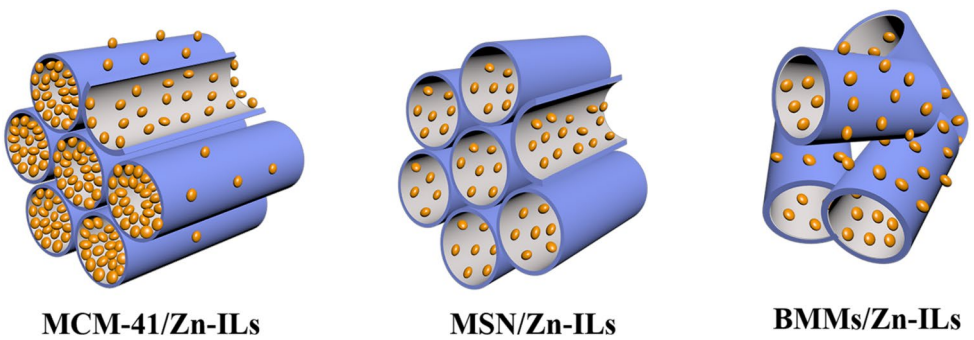

Table 4 Catalytic effect of supported ionic liquid catalyzed cycloaddition reaction

Catalyst	Yield of PC (%)	Selectivity of PC (%)
MCM-41/Zn-ILs	33	98
MSN/Zn-ILs	76	97
BMMs/Zn-ILs	77	98

Reaction condition: S/C = 200, V_{PO} = 8 mL, P_{CO2} = 1.25 MPa, T = 100 °C, t = 8 h

performances of some heterogeneous ILs catalysts were compared and listed in Table S1. Compared with a variety of other carriers, silicas as support have certain advantages and high activity, because Si–OH can not only act as a grafting point for ILs, but also a cooperative active site. In order to further study the different catalytic activities caused by varying distribution of functional groups in different supports, the effect of temperature on the cycloaddition performances was investigated (Fig. 5 and S3). The PC yields for all the catalysts were less than 30% at 80 °C after 8 h, indicating that low reaction temperature cannot offer enough energy to enhance the CO_2 cycloaddition in the fixed time. The higher catalytic activities, which are very competitive compared with many other catalysts (Table S1), were observed while increasing the reaction temperature from 80 to 120 °C, which indicates that the coupling reaction is thermodynamically favorable [46, 47]. And, on the other hand, high temperature is also conducive to the diffusion of substrate, which plays an important role in the heterogeneous catalysts. Interestingly, MSN/Zn-ILs and BMMs/Zn-ILs showed a gradually enhancement of the catalytic efficiency along with the increase of temperature, while the PC yield of MCM-41/Zn-ILs jumped by 73% as the temperature increasing from 100 to 120 °C. In other words, MSN/Zn-ILs and BMMs/Zn-ILs can obtain satisfactory activity at 100 °C, but the temperature for MCM-41/Zn-ILs must be about 120 °C. It may be explained as that MCM-41/Zn-ILs has high diffusion resistance, due to long pore channels and crowding pore entrance caused by ILs grafting, and only the active centers on the outer surface and pore entrance can be approached at low temperature. As the temperature was raised to 120 °C, the diffusion rate of substrate broke through the barrier, and the ILs inside the pore were utilized, therefore a sudden increase of the activity was observed. However, both MSN and BMMs are nanoparticle with short channel, in which the diffusion resistance of substrates is much smaller, therefore lower energy is needed. In addition, MCM-41/Zn-ILs and MSN/Zn-ILs exhibited higher catalytic efficiency than BMMs/Zn-ILs at 120 °C (Fig. S3), because the ordered pore of MCM-41/Zn-ILs and MSN/Zn-ILs favor the cooperative activation of Zn and ILs, which present much higher activity than ILs itself [48]. Obviously, short and regular channels show obvious advantages here.

The role of CO_2 pressure was studied at 100 °C and 8 h (Fig. 5 and S4). For nanoparticle catalysts of MSN/Zn-ILs and BMMs/Zn-ILs, when CO_2 pressure was increased from 0. 5 MPa to 1.25 MPa, the PC yield dramatically increased and a CO_2 pressure of 1.25 MPa resulted in the highest PC yield. These unexpected results are due to the formation of a CO_2-epoxide complex in the reaction mixture at high CO_2 pressure [49]. Since CO_2 dissolves in epoxide at high pressure, the CO_2-epoxide interactions overtake the catalyst-epoxide ones. However, for the bulky MCM-41/Zn-ILs, the CO_2 pressure showed slight influence and the best condition was 1.5 MPa, which further indicated the large diffusion resistance of the substrate in the pore is the main obstacle to its high activity.

The performances of some heterogeneous ILs catalysts were compared and listed in Table S1. Compared with a variety of other carriers, silicas as support have certain advantages and high activity, because Si–OH can not only act as a grafting point for ILs, but also a cooperative active site. And, the competitive activity has been obtained with MCM-41/Zn-ILs and MSN/Zn-ILs at the 120 °C and 1.25 MPa.

4 Conclusion

In summary, supported Zn and ILs on mesoporous silica with different morphology, including MCM-41, MSN and BMMs, as solid supports were prepared by post-grafting

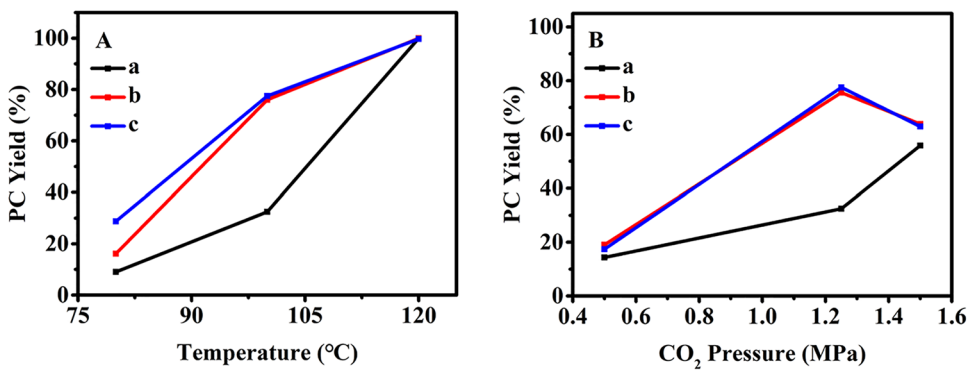

Fig. 5 Effects of temperature (**A**) and CO_2 pressure (**B**) with various catalysts **a**) MCM-41/Zn-ILs, **b**) MSN-41/Zn-ILs and **c**) BMMs/Zn-Ils

treatment. The distribution of functional groups varies in different supports: ILs in MCM-41, with bulky morphology and longer channels, blocked the pores. The functional groups in MSN, which has nanosphere morphology and order mesopores, distribute mainly inside pores. ILs in BMMs, which has wormlike mesoporous and a large number of accumulated pores, show both inside and outside the pore distribution. Then the immobilized ILs were employed as efficient catalysts for the synthesis of cyclic carbonates from CO_2 and epoxide to further study the accessibility of functional groups with varying distribution in different supports. The results showed that ILs inside mesoporous silica with shorter and ordered pore channels exhibits higher catalytic activity. Furthermore, the catalysts synthesized have many advantages, such as simple and convenient preparation method, low raw material, certain thermal stability and higher activity without additional organic solvents or co-catalysts. This work provides novel insight to improve the utilization of active sites in nanopore and further improve the activity of the immobilized catalyst.

Supplementary Information The online version contains supplementary material available at https://doi.org/10.1007/s10562-021-03667-9.

Acknowledgements This project was supported by the Beijing Municipal Natural Science Foundation (2172004), and the National Natural Science Foundation of China (21403011, 21576005).

References

1. Davis ME (2002) Ordered porous materials for emerging applications. Nature 417:813–821
2. Nugent P, Belmabkhout Y, Burd SD et al (2013) Porous materials with optimal adsorption thermodynamics and kinetics for CO_2 separation. Nature 495:80–84
3. Zhang SJ, Sun J, Zhang XC et al (2014) Ionic liquid-based green processes for energy production. Chem Soc Rev 43:7838–7869
4. Khalifeh R, Naseri V, Rajabzadeh M (2020) Synthesis of imidazolium-based ionic liquid on modified magnetic nanoparticles for application in one-pot synthesis of trisubstituted imidazoles. ChemistrySelect 5(37):11453–11462
5. Khalifeh R, Zarei Z, Rajabzadeh M (2021) Imidazolium-based ionic liquid immobilized on functionalized magnetic hydrotalcite (Fe_3O_4/HT-IM): as an efficient heterogeneous magnetic nanocatalyst for chemical fixation of carbon dioxide under green conditions. New J Chem 45(2):810–820
6. Yuan H, Wu YF, Pan XM et al (2020) Pyridyl ionic liquid functionalized ZIF-90 for catalytic conversion of CO_2 into cyclic carbonates. Catal Lett 150:3561–3571
7. Zhang P, Zhiani R (2020) Synthesis of ionic liquids as novel nanocatalysts for fixation of carbon dioxide with epoxides by using a carbon dioxide balloon. Catal Lett 150:2254–2266
8. Kim MI, Choi SJ, Kim DW et al (2014) Catalytic performance of zinc containing ionic liquids immobilized on silica for the synthesis of cyclic carbonates. J Ind Eng Chem 20:3102–3107
9. Sun J, Cheng WG, Fan W et al (2009) Reusable and efficient polymer-supported task-specific ionic liquid catalyst for cycloaddition of epoxide with CO_2. Catal Today 148:361–367
10. Kim DW, Chi DY (2004) Polymer-supported ionic liquids: imidazolium salts as catalysts for nucleophilic substitution reactions including fluorinations. Angew Chem Int Ed 43:483–485
11. Zhang WH, He PP, Wu S et al (2016) Graphene oxide grafted hydroxyl-functionalized ionic liquid: a highly efficient catalyst for cycloaddition of CO_2 with epoxides. Appl Catal A 509:111–117
12. Lan DH, Chen L, Au CT et al (2015) One-pot synthesized multifunctional graphene oxide as a water-tolerant and efficient metal-free heterogeneous catalyst for cycloaddition reaction. Carbon 93:22–31
13. Ding YS, Guo CY, Dong JY et al (2006) Novel organic modification of montmorillonite in hydrocarbon solvent using ionic liquid-type surfactant for the preparation of polyolefin-clay nanocomposites. J Appl Polym Sci 102:4314–4320
14. Rezaei F, Amrollahi MA, Khalifeh R (2019) Design and synthesis of Fe_3O_4@SiO_2/aza-crown ether-Cu(II) as a novel and highly efficient magnetic nanocomposite catalyst for the synthesis of 1, 2, 3-triazoles, 1-substituted 1H-tetrazoles and 5-substituted 1H-tetrazoles in green solvents. Inorg Chim Acta 489:8–18
15. Rajabzadeh M, Khalifeh R, Eshghi H et al (2019) Design and preparation of hallow mesoporous silica spheres include CuO and its catalytic performance for synthesis of 1, 2, 3-triazole compounds via the click reaction in water. Catal Lett 149(4):1125–1134
16. Rajabzadeh M, Khalifeh R, Eshghi H et al (2020) Design and synthesis of CuO@SiO_2 multi-yolk@shell and its application as a new catalyst for CO_2 fixation reaction under solventless condition. J Ind Eng Chem 89:458–469
17. Hoffmann F, Cornelius M, Morell J et al (2006) Silica-based mesoporous organic-inorganic hybrid materials. Angew Chem Int Ed 45:3216–3251
18. Pal N, Bhaumik A (2015) Mesoporous materials: versatile supports in heterogeneous catalysis for liquid phase catalytic transformations. RSC Adv 5:24363–24391
19. Mcmorn P, Hutchings GJ (2004) Heterogeneous enantioselective catalysts: strategies for the immobilisation of homogeneous catalysts. Chem Soc Rev 33:108–222
20. Song CE, Lee SG (2002) Supported chiral catalysts on inorganic materials. Chem Rev 102:3495–3524
21. Lagarde F, Srour H, Berthet N et al (2019) Investigating the role of SBA-15 silica on the activity of quaternary ammonium halides in the coupling of epoxides and CO_2. J CO2 Util 34:34–39
22. Han L, Park SW, Park DW (2009) Silica grafted imidazolium-based ionic liquids: efficient heterogeneous catalysts for chemical fixation of CO_2 to a cyclic carbonate. Energy Environ Sci 2:1286–1292
23. Sakai T, Tsutsumi Y, Ema T (2008) Highly active and robust organic-inorganic hybrid catalyst for the synthesis of cyclic carbonates from carbon dioxide and epoxides. Green Chem 10:337–341
24. He X, Bai SY, Sun JH et al (2018) Bipyridine-proline grafted silicas with different mesopore structures: their catalytic performance in asymmetric aldol reaction and structure effect. Catal Lett 148:2408–2417
25. Hukkamäki J, Suvanto S, Suvanto M et al (2004) Influence of the pore structure of MCM-41 and SBA-15 silica fibers on atomic layer chemical vapor deposition of cobalt carbonyl. Langmuir 20:10288–10295
26. Zhu ZJ, Bai SY, Shang H et al (2020) One-pot assembling of hierarchical porous carbon/silica nanocomposites for cycloaddition reaction. Microporous Mesoporous Mater 293:109768
27. Khalifeh R, Sorouri M, Damirchi EK et al (2020) Efficient and selective CO_2 and CS_2 conversion to cyclic carbonates and trithiocarbonates by using multishell hollow $CoAl_2O_4$ microsphere as a unique catalyst under solventless condition. J Taiwan Inst Chem Eng 115:229–241

28. Pourhassan F, Khalifeh R, Eshghi H (2021) Well dispersed gold nanoparticles into the multi amine functionalized SBA-15 for green chemical fixation of carbon dioxide to cyclic carbonates under solvent free conditions. Fuel 287:119567
29. Khalifeh R, Karimi M, Rajabzadeh M et al (2020) Synthesis and morphology control of nano $CuAl_2O_4$ hollow spheres and their application as an efficient and sustainable catalyst for CO_2 fixation. J CO2 Util 41:101233
30. Kresge CT, Leonowicz ME, Roth WJ et al (1992) Ordered mesoporous molecular sieves synthesized by liquid-crystal template mechanism. Nature 359:710–712
31. Bhattacharyya S, Wang H, Ducheyne P (2012) Polymer-coated mesoporous silica nanoparticles for the controlled release of macromolecules. Acta Biomater 8:3429–3435
32. Sun JH, Shan ZP, Maschmeyer T et al (2003) Synthesis of bimodal nanostructured silicas with independently controlled small and large mesopore sizes. Langmuir 19:8395–8402
33. Xu J, Wu HT, Ma CM et al (2013) Ionic liquid immobilized on mesocellular silica foam as an efficient heterogeneous catalyst for the synthesis of dimethyl carbonate via transesterification. Appl Catal A 464–465:357–363
34. Shang H, Bai SY, Yao J et al (2020) Bifunctional catalysts containing Zn(II) and imidazolium salt ionic liquids for chemical fixation of carbon dioxide. Chem Asian J 16:224–231
35. Bai SY, Hu XT, Sun JH et al (2014) Preparation and characterization of Ti supported bimodal mesoporous catalysts using a self-assembly route combined with a ship-in-a-bottle method. New J Chem 38:2128–2134
36. Emmeluth C, Suhm MA, Luckhaus D (2003) A monomers-in-dimers model for carboxylic acid dimers. J Chem Phys 118:2242–2255
37. Kruk M, Jaroniec M (2001) Gas adsorption characterization of ordered organic-inorganic nanocomposite materials. Chem Mater 13:3169–3183
38. Sing KSW, Everett DH, Haul RAW et al (1985) Reporting physisorption data for gas/solid systems. Pure Appl Chem 57:603–619
39. Udayakumar S, Pandurangan A, Sinha PK (2005) Mesoporous material as catalyst for the production of fine chemical: synthesis of dimethyl phthalate assisted by hydrophobic nature MCM-41. J Mol Catal A Chem 240:139–154
40. Slowing I, Trewyn BG, Lin VSY (2006) Effect of surface functionalization of MCM-41-type mesoporous silica nanoparticles on the endocytosis by human cancer cells. J Am Chem Soc 128:14792–14793
41. Pająk L, Jarzębski AB, Mrowiec-bialoń J et al (2000) SAXS studies on porous inorganic dry gels. Proc SPIE 4240:74–80
42. de Moor PPEA, Beelen TPM, van Santen RA (1997) SAXS/WAXS study on the formation of precursors and crystallization of silicalite. Microporous Mater 9:117–130
43. Boukari H, Lin JS, Harris MT (1997) Probing the dynamics of the silica nanostructure formation and growth by SAXS. Chem Mater 9:2376–2384
44. Luo ZQ, Wang J, He YQ et al (2020) A stable Zn-based metal-organic framework as an efficient catalyst for carbon dioxide cycloaddition and alcoholysis at mild condition. Catal Lett 150:1408–1417
45. Qin L, Ji YY, Ding T et al (2020) Poly(ionic liquid)s-supported N-heterocyclic carbene silver complexes for the cycloaddition of CO_2 with epoxides. Catal Lett 150:1196–1203
46. Wei RJ, Zhang XH, Du BY et al (2013) Synthesis of bis(cyclic carbonate) and propylene carbonate via a one-pot coupling reaction of CO_2, bisepoxide and propylene oxide. RSC Adv 3:17307–17313
47. Song JL, Zhang BB, Zhang P et al (2012) Highly efficient synthesis of cyclic carbonates from CO_2 and epoxides catalyzed by KI/lecithin. Catal Today 183:130–135
48. Yang ZZ, Zhao YN, He LN (2011) CO_2 chemistry: task-specific ionic liquids for CO_2 capture/activation and subsequent conversion. RSC Adv 1:545–567
49. Yue S, Wang PP, Hao XY (2019) Synthesis of cyclic carbonate from CO_2 and epoxide using bifunctional imidazolium ionic liquid under mild conditions. Fuel 251:233–241